VERSITA

Acta Geophysica
vol. 60, no. 3, Jun. 2012, pp. 638-663
DOI: 10.2478/s11600-011-0069-2

A Statistical Damage Model with Implications for Precursory Seismicity

Ya-Ting LEE[1,2], Donald L. TURCOTTE[2], John B. RUNDLE[2,3], and Chien-Chih CHEN[1]

[1]Graduate Institute of Geophysics, National Central University, Jhongli, Taiwan
e-mails: shine2530@gmail.com (corresponding author), chencc@earth.ncu.edu.tw

[2]Department of Geology, University of California, Davis, CA, USA
e-mails: dlturcotte@ucdavis.edu, jbrundle@ucdavis.edu

[3]Department of Physics, University of California, Davis, CA, USA

Abstract

Acoustic emissions prior to rupture indicate precursory damage. Laboratory studies of frictional sliding on model faults feature accelerating rates of acoustic emissions prior to rupture. Precursory seismic emissions are not generally observed prior to earthquakes. To address the problem of precursory damage, we consider failure in a fiber-bundle model. We observe a clearly defined nucleation phase followed by a catastrophic rupture. The fibers are hypothesized to represent asperities on a fault. Two limiting behaviors are the equal load sharing $p = 0$ (stress from a failed fiber is transferred equally to all surviving fibers) and the local load sharing $p = 1$ (stress from a failed fiber is transferred to adjacent fibers). We show that precursory damage in the nucleation phase is greatly reduced in the local-load sharing limit. The local transfer of stress from an asperity concentrates nucleation, restricting precursory acoustic emissions (seismic activity).

Key words: earthquake precursors, acoustic emissions, fiber-bundle model, rupture, nucleation.

1. INTRODUCTION

A magnitude $M_w = 6.0$ earthquake occurred on the Parkfield segment of the San Andreas fault on 28 September 2004. This was the most recent in a sequence of $M \approx 6.0$ earthquakes that have occurred on this segment with mean intervals of about 30 years. In expectation of this event, a dense array of instruments were deployed to study all aspects of the earthquake. Seismometers were installed to monitor any precursory seismic activity. No precursory seismic activity was observed on or near the rupture surface. The instrument sensitivity extended down to at least an $M = 1$ earthquake (Bakun *et al*. 2005).

The object of this paper is to study the physical processes responsible for precursory seismicity. Two examples of precursory seismicity have received considerable attention. The first of these are foreshocks. Extensive statistical studies have shown that the magnitudes of most foreshocks are very nearly as large as the subsequent mainshocks (Savage and dePolo 1993). In addition, the times of occurrence of the foreshocks are quite close to the times of the mainshocks (Agnew and Jones 1991). These observations have led to the working hypothesis that a foreshock is an aftershock that had a magnitude larger than the magnitude of the original mainshock (Helmstetter and Sornette 2003). About 5% of earthquakes have foreshocks (Reasenberg 1999). No foreshocks occurred prior to the 2004 Parkfield earthquake.

A second example of observed precursory seismicity is accelerated moment release (AMR) (Bowman *et al*. 1998). There is considerable evidence that there may be an increase in the number of intermediate-sized earthquakes prior to some large earthquakes. This precursory seismicity occurs over periods of years and accelerates in frequency prior to the large earthquake. The region over which this seismicity occurs appears to scale as a correlation length which is a function of the magnitude of the large earthquake. Earthquakes associated with foreshocks and AMR occur on faults other than the fault on which the subsequent large earthquake occurs. In this paper our concern is the occurrence of precursory seismicity on the fault zone on which a large earthquake subsequently occurs. No such seismicity was observed prior the 2004 Parkfield earthquake. We propose a model for the physics of material failure associated with an earthquake.

Our understanding of the physics of material failure is largely based on laboratory experiments. The Parkfield earthquake occurred on a well defined fault, the San Andreas, that had been subject to many previous ruptures. It is generally hypothesized that fault ruptures occur when the applied shear stress exceeds the "static" coefficient of friction. Many laboratory studies of frictional sliding on model faults have been carried out (Marone 1998). Probably the most relevant in terms of precursory damage prior to failure was carried out by Weeks *et al*. (1978). A large granite block containing

a through-going saw cut was confined at pressures up to 100 MPa. Under constant stress-rate loading, fourteen violent slip events occurred. Some 8000 microseismic events also occurred. A systematic increase in the rate of microseismic events was observed prior to each major slip event. These events satisfied a power-law frequency-amplitude scaling to a good approximation.

The granite blocks constituted rigid elastic half spaces with near uniform properties. The frictional resistance of the saw cut can be attributed to "asperities" (points of contact) across the saw cut. These asperities can be assumed to have a range of scales and strengths. When an asperity fails, the stress carried by the asperity is transferred to other asperities. The physics of this stress transfer is a major focus of this paper. The precursory acoustic emissions can be associated with failure of weak "asperities" (points of contact). A major question in earthquake physics is: Why do we not observe asperity failures (small earthquakes) prior to an event such as the Parkfield earthquake?

Before presenting our model for earthquake rupture it is appropriate to discuss the relevance of these laboratory studies to earthquake ruptures. It is generally accepted that friction is the applicable rheology for faults. However, there are differences between the laboratory conditions and the conditions of a fault. In the laboratory, normal stresses are much lower and the rates of strain are much higher. In addition, the role of fluids in terms of fluid pressure and chemical healing of a fault are not duplicated. Thus caution must be exercised in relating the laboratory experiments to earthquakes.

In this paper we restrict our earthquake discussion to the precursory behavior prior to the 2004 Parkfield earthquake because of the very sensitive seismic network adjacent to the rupture which provides the best available evidence for the absence of precursory small earthquakes. We have restricted our discussion of laboratory experiments to those of Weeks *et al*. (1978) because they most closely simulate the earthquake rupture.

The basic observation we address in this paper is the absence of small earthquakes on a fault prior to a large earthquake. This is not the case for the laboratory experiments discussed above, in which a large number of microseismic events preceded rupture. In order to provide an answer to this question, we will consider a discrete model for the behavior of asperities on a rupture surface. Several discrete models for faults have been proposed. The first large-scale model was studied by Carlson and Langer (1989). These authors considered a long linear array of slider blocks; each block was attached to a constant velocity driver plate by loader springs, spring constant K_L, and was connected to the two adjacent blocks with connector springs, spring constant K_c. They used a velocity weakening friction law and considered up to 400 blocks. Slip events involved various numbers of blocks. The frequency-size distribution of events was found to satisfy power-law scaling. Many

other slider-blocks simulations have been carried out with similar results. This work has been reviewed by Turcotte (1999). A near uniform behavior is found under a wide range of conditions. This behavior is controlled by the ratio of spring constants

$$\gamma = \frac{K_C}{K_L} . \tag{1}$$

If γ is very small, single block failures dominate; as γ is increased a power-law frequency-size distribution of small events develops but no large events occur. The ratio of spring constants γ can be increased until the power-law distribution extends across the entire array; this is taken to be a critical point, and γ is the turning parameter. As γ is increased further, system wide events occur with a power-law distribution of small events. In the limit $\gamma \to \infty$ only system wide events occur (Turcotte *et al*. 2007). There are similarities between the large γ slider-block model and the experiments described above. However, a systematic acceleration of small slip events prior to a large event is not seen.

In this paper we will model fault rupture using a fiber-bundle model. We associate the fibers with asperities on a fault. We will consider in some detail the relation of the fiber-bundle model to the slider-block model in the Appendix. Fiber-bundle models have been widely used to model material failure (Pradhan *et al*. 2010), specifically for composite materials. Two types of fiber-bundle models have been proposed. The first is a static model in which the failure strength of each fiber is specified from a statistical distribution (Daniels 1945). There is no time dependence in this model, a fiber fails instantaneously when the stress on the fiber is equal to or greater than the prescribed failure strength. The second type of model is dynamic and time dependent. A time to failure is specified for each fiber from a statistical distribution. These failure times are strongly stress dependent (Coleman 1958).

It is also necessary to specify how the stress from a failed fiber is redistributed to other fibers. One extreme case is an equal load sharing. The stress from a failed fiber is redistributed equally to all surviving fibers. The other extreme case is a local load sharing. The stress from a failed fiber is redistributed equally to adjacent fibers. Fiber-bundle models have been reviewed by Phoenix and Newman (2009).

An important distinction between slider-block and fiber-bundle models is healing. In the standard slider-block model, the surface heals after a slip event and multiple slip events involving a block can occur. In the standard fiber-bundle model, the fiber is removed from the system when it fails and cannot carry a stress again.

Our objective is to model the failure of asperities on a fault during stress accumulation. We make the hypothesis that when an asperity fails it does not

restick and therefore we utilize the fiber-bundle model in preference to the slider-block model. Since stress accumulation on a fault is a slow process we choose the static model and specify the distribution of the strengths of the fibers (asperities). We find the variability of these strengths (coefficient of variation representing material heterogeneity) to be an important parameter. Redistribution of stress from a failed fiber is also important. Two extremes are the uniform load sharing (the load is redistributed uniformly to surviving fibers) and the local load sharing (load is redistributed to adjacent fibers). We associate the near uniform load sharing with the laboratory experiments described above due to the rigidity of the granite matrix. We associate the local load sharing with actual faults due to the damaged matrix in which they are embedded. We will show that precursory failures are fewer with local load sharing than with uniform load sharing.

There have been extensive discussions in the physics literature whether the transition from nucleation to rupture is a phase change. This work has been reviewed by Alava *et al*. (2006) and Pradhan *et al*. (2010). The thermodynamics of fiber-bundle models has been discussed by Pride and Toussaint (2002). Central to this work is the definition of temperature for the problem. Fluctuations can be introduced but they do not follow naturally from the basic fiber-bundle model.

A relevant set of laboratory experiments have been carried out by Garcimartin *et al*. (1997) and by Guarino *et al*. (1998, 1999, 2002). These authors studied the failure of circular panels (222 mm diameter, 3-5 mm thickness) of chipboard. A differential pressure across the panel was (1) increased linearly in time until failure occurred, or (2) increased instantaneously and held constant until failure occurred. The use of chipboard introduced a relatively soft material with interacting fibers similar to our fault model. Precursory micro fractures occurred. Initially, the micro fractures occurred randomly but they subsequently coalesced in the region of subsequent rupture initiation. Precursory acoustic emissions occurred similar in form to those illustrated in Fig. 4b. We conclude that the near uniform tension hoop stresses in the panels result in a near uniform stress distribution from failed fibers.

Scorretti *et al*. (2001) and Ciliberto *et al*. (2001) discussed the failure behavior of the chipboard in terms of a fiber-bundle model. They argued that the dominant feature is a random (thermal) distribution of stresses. The heterogeneous stress field is not due to thermalization but rather due to the stress interactions in the heterogeneous chipboard. Their explanation would appear also applicable to earthquakes on faults. The heterogeneous nature of the earth's crust due to distribution of faults and joints on all scales leads to a strongly heterogeneous stress field. This heterogeneous stress field masks the build up of stress during the tectonic earthquake cycle, as discussed above.

2. FIBER-BUNDLE MODEL

Our model consists of a square array of n_0 fibers, as illustrated in Fig. 1. A load F_0 is applied to the array and the mean stress on the fibers $\overline{f}$ is given by

$$\overline{f} = \frac{F}{n_0} \,. \tag{2}$$

The failure force for each fiber i, f_{fi}, is specified by a statistical distribution of failure forces. Based on many studies, we choose the Weibull distribution (Weibull 1951, Meeker and Escobar 1998). The unique property of the Weibull distribution is the scale-invariant, power-law behavior of its hazard function. The cumulative distribution function (cdf) for this distribution is given by

$$P\left(f_{fi}\right) = 1 - \exp\left[-\left(\frac{f_{fi}}{f_0}\right)^{\beta}\right], \tag{3}$$

where f_0 is a reference failure force and β is the power-law exponent. The mean $\overline{f}$, standard deviation σ, and coefficient of variation C_v of the Weibull distribution are given by

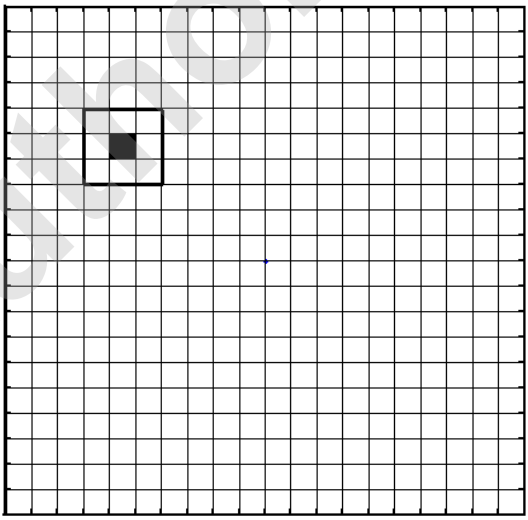

Fig. 1. Illustration of the model. A square array of fibers is considered with L fibers on a side. For the example shown $L = 20$ so the original number of fibers is $n_0 = 20^2 = 400$. The load on the fibers is increased until the weakest fiber fails, this is indicated by the solid square. A local load sharing region is defined, for the case illustrated $r = 1$ and the number of fibers in this region is n_{rd} 8 as given by Eq. (7).

$$\overline{f} = f_0 \Gamma\left(1+1/\beta\right) , \tag{4}$$

$$\sigma = f_0 \left\{ \Gamma\left(1+2/\beta\right) - \left[\Gamma\left(1+1/\beta\right)\right]^2 \right\}^{1/2} , \tag{5}$$

$$C_v = \frac{\sigma}{\overline{f}} = \left\{ \frac{\Gamma\left(1+2/\beta\right)}{\left[\Gamma\left(1+1/\beta\right)\right]^2} - 1 \right\}^{1/2} . \tag{6}$$

When $\beta = 1$, the Weibull distribution reduces to the exponential distribution. In the limit $\beta \to \infty$ all fibers fail at the reference failure force f_0. The applicability of the Weibull distribution to the failure of fibers has been established directly by experimental studies (Pradhan *et al*. 2010).

We determine the failure strength of the fibers is in our fiber bundle randomly. For each fiber, a random number P_i in the range 0 to 1 is chosen. Using this random number, the failure force f_{fi}/f_0 is obtained from Eq. (3). The first fiber fails at $f_{fi} = f_{f\min}$, the smallest failure stress. The force on the array is increased until $f = f_{f\min}$, and the weakest fiber fails. The failed fiber is removed from the array and the force on this fiber $f_{f\min}$ is redistributed onto the surviving fibers, the total force on the array F remains constant.

The redistributed force is divided into two parts. A fraction p is redistributed equally to all surviving fibers within a range of interaction r (Kun *et al*. 2000). The parameter p is a measure of the stiffness of the system. A stiff system has p near zero and a soft system has p near unity. If the medium in which a fault is embedded behaves elastically then the stress is redistributed according to the laws of elasticity. However, actual faults are embedded in a damaged region. Transfers of stress induce displacements on the ensemble of embedded faults. The result is that the matrix is relatively soft.

The concept of local load shearing is illustrated in Fig. 1 with $r = 1$. This local load sharing is carried out over a square region with $2r + 1$ fibers on a side. The number of fibers n_{rd} over which this fraction of the failed load is redistributed is

$$n_{rd} = \left(2r+1\right)^2 - 1 . \tag{7}$$

For example, in Fig. 1, $n_{rd} = 8$. Each of these n_{rd} fibers has an increase in force Δf_{lls} given by

$$\Delta f_{lls} = \frac{p f_{f\min}}{n_{rd}} . \tag{8}$$

In subsequent redistributions, some of the fibers in the local load sharing region may have been removed due to previous failures. In this case, the stress is redistributed to the surviving fibers. In terms of the fiber-bundle model, local load sharing takes into account the frictional transfer of stress to adjacent fibers when a fiber fails.

The other redistribution fraction $(1-p)$ is distributed equally to all surviving fibers. This is uniform load sharing. For the failure of the first fiber each of the $n_0 - 1$ surviving fibers has an increase in force Δf_{els} given by

$$\Delta f_{els} = \frac{(1-p) f_{f\min}}{(n-1)} . \tag{9}$$

The fibers within the square local load sharing region receive both contributions. The limit $p = 0$ is the uniform load sharing. A fiber does not interact with other fibers and when it fails its stress is redistributed equally to all other fibers. This equal redistribution of stresses would be appropriate for the granite block experiments carried out by Weeks *et al*. (1978) and discussed above. This would be a very stiff system. In order to specify our problem we require: (1) array size n_0, (2) range of interaction r, (3) measure of load sharing p, and (4) Weibull exponent β. As a measure of the applied load we consider the mean load per original fiber as given in Eq. (2). We further assume that the applied load $F(t)$ increases linearly with time t and write

$$\overline{f} = f_0 \frac{t}{t_0} , \tag{10}$$

where t_0 is a reference time and f_0 is the reference failure force introduced in Eq. (3).

3. MEAN-FIELD SOLUTION

To illustrate our fiber-bundle model we first consider the mean-field (uniform-load sharing) limit $p = 0$. In this case we can obtain an analytic solution. In the mean-field limit, the forces $f(t)$ on the surviving fibers are equal. The number of surviving fibers is $n(t)$. From Eq. (3) we note that in the limit $\beta \to \infty$ all fibers fail at the reference fiber load f_0. Thus from Eq. (10) we see that the failure of the array in this limit occurs at $t = t_0$. We will obtain our solutions as a function of the nondimensional time t/t_0.

In order to quantify the failure of our fiber bundle we introduce the concept of damage mechanics (Krajcinovic 1996). The damage variable α is defined by

$$E = E_0(1-\alpha) , \tag{11}$$

where E is Young's modulus during failure and E_0 is the original reference value of Young's modulus. The damage variable α quantifies the deviation from linear elasticity due to damage such as microcracks. For our fiber-bundle array with equal load sharing we have

$$\alpha = 1 - \frac{n}{n_0} . \tag{12}$$

This follows from the relation

$$E = E_0 \frac{n}{n_0} . \tag{13}$$

A primary objective of our studies is to obtain $\alpha(t/t_0)$.

We first write a force balance for the array with equal-load sharing. This is given by

$$F = n_0 \overline{f} = nf . \tag{14}$$

Since the fiber force f is the same for all fibers, the number of surviving fibers is related to the fiber force by Eq. (3) with the result

$$\frac{n}{n_0} = \exp\left[-\left(\frac{f}{f_0} \right)^{\beta} \right] . \tag{15}$$

Combining Eqs. (10) and (14) gives

$$\frac{\overline{f}}{f_0} = \frac{f}{f_0} \frac{n}{n_0} = \frac{t}{t_0} . \tag{16}$$

Combining this with Eq. (16) gives

$$\frac{t}{t_0} = \frac{f}{f_0} \exp\left[-\left(\frac{f}{f_0} \right)^{\beta} \right] . \tag{17}$$

This equation gives f/f_0 as a function of t/t_0. It is important to note that for each value of t/t_0 there are two values of f/f_0. This will be illustrated below. From Eqs. (12) and (16) we have

$$\alpha = 1 - \frac{n}{n_0} = 1 - \frac{t}{t_0} \frac{f_0}{f} , \tag{18}$$

which can be used to obtain α as a function of t/t_0. The dependence of α on t/t_0 is given in Fig. 2 for $\beta = 2$, 6, and 10. We see that the damage increases slowly to a maximum critical value of α, α_c, at which time, t_c, the total failure occurs catastrophically. The increase in damage from $\alpha = 0$ at $t = 0$ to $\alpha = \alpha_c$ at $t = t_c$ is a nucleation phase and the increase in damage from $\alpha = \alpha_c$ to $\alpha = 1$ at $t = t_c$ is a rupture phase. This transition can be associated with a second-order phase change since $\mathrm{d}\alpha/\mathrm{d}t$ is continuous but $\mathrm{d}^2\alpha/\mathrm{d}t^2$ is discontinuous. As noted above, there are two values of α for each value of t/t_0. The upper values shown as dashed lines are not physical. When $\mathrm{d}\alpha/\mathrm{d}t \to \infty$ the value of α increases instantaneously, as shown by the solid lines in Fig. 2.

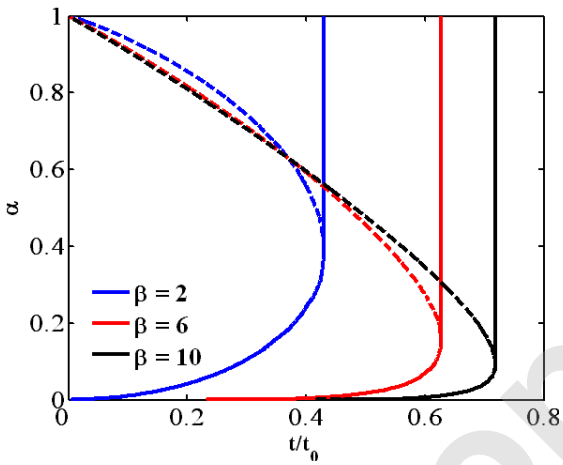

Fig. 2. The dependence of the damage variable α on the nondimensional time t/t_0 in the uniform load sharing (mean field) limit with $\beta = 2$, 6, and 10. The transition from the nucleation phase to the rupture phase occurs when $d\alpha/dt \to \infty$ with $\alpha = \alpha_c$ and $t = t_c$. The vertical lines represent the rupture phase, the dashed lines are solutions of Eq. (18) but are not physical.

We can obtain simple analytic expressions for the critical failure time t_c and the corresponding value of damage α_c. As can be seen in Fig. 2 we have $d\alpha/dt = \infty$ at this critical point. This corresponds to the condition $df/dt = \infty$ or $dt/df = 0$. Taking the derivative of Eq. (17) we obtain

$$\frac{f_0}{t_0}\frac{dt}{df} = \exp\left(-\frac{f}{f_0}\right)^{\beta}\left[1-\beta\left(\frac{f}{f_0}\right)^{\beta}\right] = 0 \ , \tag{19}$$

which gives

$$\frac{f_c}{f_0} = \left(\frac{1}{\beta}\right)^{1/\beta} \ . \tag{20}$$

And from Eq. (17) we have

$$\frac{t_c}{t_0} = \left(\frac{1}{\beta}\right)^{\frac{1}{\beta}} \exp\left(-\frac{1}{\beta}\right) . \tag{21}$$

Combining Eqs. (18), (20), and (21) gives

$$\alpha_c = 1 - \exp\left(-\frac{1}{\beta}\right) . \tag{22}$$

For the examples considered in Fig. 2 we have for $\beta = 2$, 6, and 10, $f_c/f_0 = 0.707$, 0.742, and 0.794; $t_c/t_0 = 0.429$, 0.628, and 0.719; and $\alpha_c = 0.393$, 0.154, and 0.095.

Although we have a critical failure of the array, we do not have a propagating fracture. In the equal load sharing (mean field) limit failures are spatially random. There is no localization and nucleation of a propagating rupture.

It is also of interest to determine the energy dissipated by fiber failure. We assume that the energy dissipated is the elastic energy in the fiber just prior to failure. We associate this energy with acoustic emissions and seismic energy. Our objective is to determine the time dependence of the dissipated energy during the nucleation phase and the relative magnitudes of energy dissipated during the nucleation phase and the rupture phase.

We will again define a reference failure energy E_0 in the limit $\beta \to \infty$. In this limit all fibers fail at the reference fiber load f_0. The energy dissipated when a fiber fails at this load e_0 is given by the elastic energy in the fiber at this load

$$e_0 = \frac{A_f L_f \sigma_0^2}{2E_f} , \tag{23}$$

where A_f is the fiber area, L_f is the fiber length, E_f is Young's modulus of the fiber, and σ_0 is the fiber failure stress. Using the relation

$$f_0 = A_f \sigma_0 . \tag{24}$$

Equation (23) can be written as

$$e_0 = \frac{L_f f_0^2}{2A_f E_f} . \tag{25}$$

The total energy associated with the failure of the fiber bundle in the limit $\beta \to \infty$, E_0 is given by

$$E_0 = n_0 e_0 = \frac{A_f L_f \sigma_0^2 n_0}{2E_f} . \tag{26}$$

The energy dissipated when a fiber fails at the load f is given by

$$e_f = \frac{L_f f^2}{2A_f E_f} . \tag{27}$$

Using Eqs. (25) and (27) we introduce the nondimensional failure energy

$$\frac{e_f}{e_0} = \left(\frac{f}{f_0} \right)^2 . \tag{28}$$

We now apply this result to our mean-field fiber bundle failure. In this case all fibers have the same force $f(t)$. We next determine the cumulative energy E dissipated in the fiber bundle as it fails. We consider the nondimensional ratio E/E_0 which is given by

$$\frac{E}{E_0} = \frac{1}{n_0}\int_{t=0}^{t/t_0} \frac{e_f}{e_0}\,\mathrm{d}n \,. \tag{29}$$

Taking the derivative of Eq. (15) we obtain

$$\frac{1}{n_0}\frac{\mathrm{d}n}{\mathrm{d}(f/f_0)} = \beta\left(\frac{f}{f_0}\right)^{\beta-1} \exp\left[-\left(\frac{f}{f_0}\right)^{\beta}\right]. \tag{30}$$

Substitution of Eqs. (28) and (30) into Eq. (29) gives

$$\frac{E}{E_0} = \beta\int_0^{f/f_0}\left(\frac{f}{f_0}\right)^{\beta+1} \exp\left[-\left(\frac{f}{f_0}\right)^{\beta}\right]\mathrm{d}\left(\frac{f}{f_0}\right). \tag{31}$$

Making the substitution

$$s = \left(\frac{f}{f_0}\right)^{\beta} \,. \tag{32}$$

Equation (31) can be written as

$$\frac{E}{E_0} = \beta\int_0^{(f/f_0)^{\beta}} s^{\frac{2}{\beta}} e^{-s}\mathrm{d}s = \beta\gamma\left[\left(\frac{2}{\beta}+1\right), \left(\frac{f}{f_0}\right)^{\beta}\right], \tag{33}$$

where γ is the lower incomplete gamma function (Abramowitz and Stegun 1972).

From Eqs. (17) and (31) we obtain E/E_0 as a function of t/t_0.

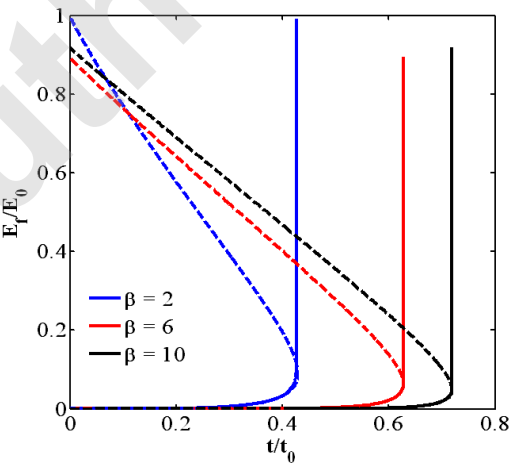

Fig. 3. Dependence of the nondimensional accumulative energy dissipated E_f/E_0 on the nondimensional time $t = t_0$ in the uniform load sharing (mean field, $p = 0$) limit with $\beta = 2$, 6, and 10. The transition from the nucleation phase to the rupture phase occurs when $\mathrm{d}E_f/\mathrm{d}t \to \infty$ with $E_f = E_n$ and $t = t_c$. The vertical lines represent the rupture phase, the dashed lines are solutions of Eq. (17) and (31) but are not physical.

The dependence of the cumulative energy dissipated E/E_0 on t/t_0 is given in Fig. 3 for $\beta = 2$, 6, and 10. The nucleation and rupture phases are clearly illustrated. The energy dissipated during the nucleation phase E_n is associated with precursory fiber failures or foreshocks. The energy dissipated during the rupture phase E_r is associated with the propagating rupture or main shock. For $\beta = 2$ we have $E_n/E_0 = 0.097$ and $E_r/E_0 = 0.893$ so that $E_n/E_r = 0.109$, about 10% of the energy is dissipated in the nucleation phase. For $\beta = 6$ the values are $E_n/E_0 = 0.064$, $E_r/E_0 = 0.830$, and $E_n/E_r = 0.072$. For $\beta = 10$ we have $E_n/E_0 = 0.049$, $E_r/E_0 = 0.870$, and $E_n/E_r = 0.056$.

4. SIMULATIONS

In order to understand the behavior of our model we have carried out a sequence of numerical simulations. All simulations are carried out on a square array of width 150 so that the original number of fibers is $n_0 = 150^2 = 22\,500$. Our simulations will also be restricted to the range of interaction $r = 1$. Results will be given for power-law exponents $\beta = 2$, 6, and 10 and a range of values of the redistribution parameter p. Varying the range of interaction r gives results similar to those obtained by varying the redistribution parameter p.

In Figure 4 nucleation and propagation of the rupture are illustrated for several typical examples. The distributions of failed fibers (dark areas) are given for increasing values of the damage variable. The lowest value of the damage variable, $\alpha = 0.07$ in Fig. 4a, is during the nucleation phase. The second value of the damage variable, $\alpha_c = 0.145$ in Fig. 4a, is at the critical transition from nucleation to rupture. The largest value of the damage variable, $\alpha = 0.3$ in Fig. 4a, is during the propagation phase. Note that periodic boundary conditions are assumed so that when the propagating fracture reaches the top boundary of the array its extension appears at the lower boundary. The amount of damage during the nucleation phase decreases with increasing value of p and β.

It is also of interest to study the distribution of cluster areas at the critical transition from nucleation to propagation. In Figure 5 we give the cumulative number of clusters N_{cc} with areas greater than A_c for the four examples given in Fig. 4. The cluster area A_c is taken to be the number of adjacent fibers that have failed. We compare our data in Fig. 5 with the power-law scaling relation

$$N_{cc} = CA_c^{-D/2} \quad . \tag{34}$$

We find quite good scaling taking the fractal dimension $D = 4$. Hemmer and Hansen (1992) found a similar dependence for their fiber bundle studies taking $D = 3$.

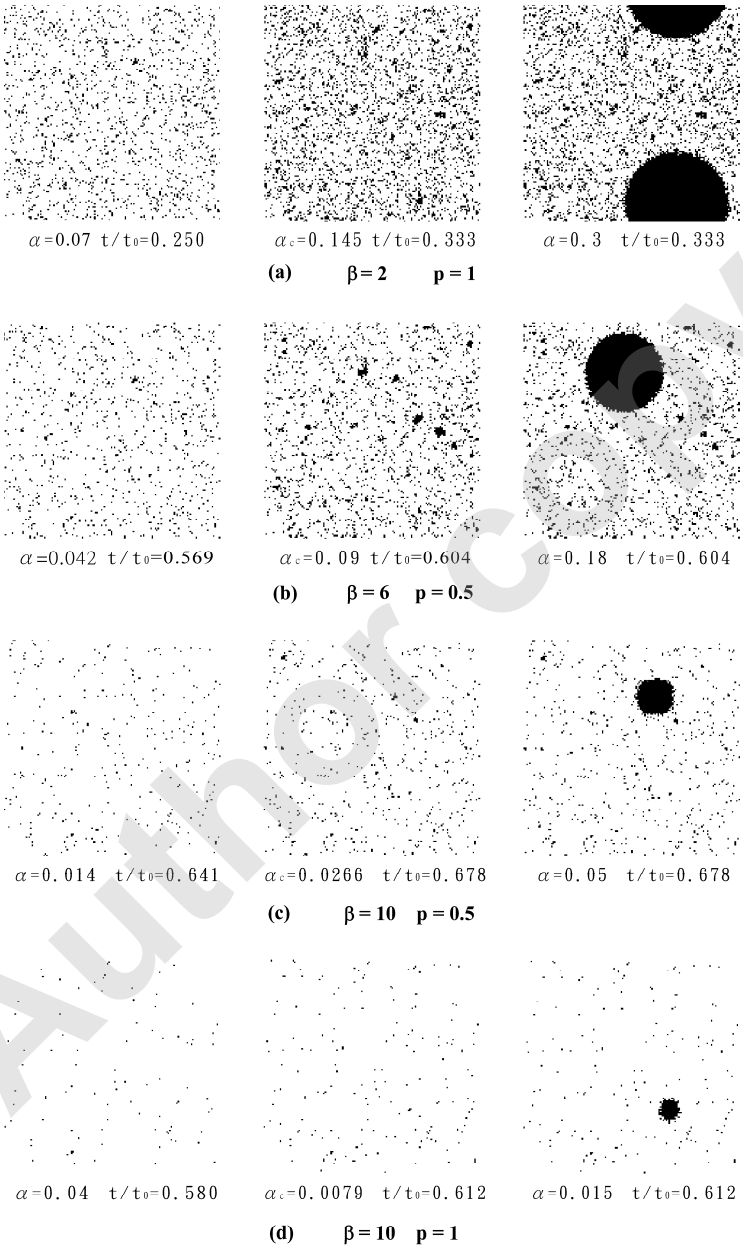

Fig. 4. Four examples of rupture nucleation and propagation are illustrated. The dark regions are failed fibers. On the left are examples during nucleation, on the center critical ($\alpha = \alpha_c$) nucleation is illustrated and on the right are examples during rupture. In all cases $n_0 = 22\,500$ and $r = 1$. Results are given for: (a) $\beta = 2$, $p = 1$, (b) $\beta = 6$, $p = 0.5$, (c) $\beta = 10$, $p = 0.5$, and (d) $\beta = 10$, $p = 1$.

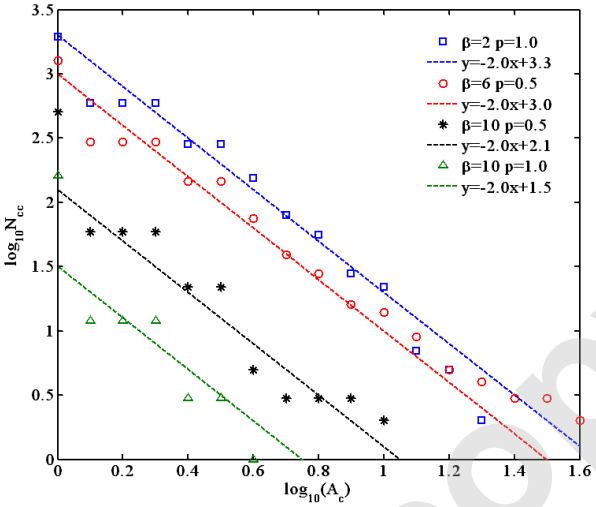

Fig. 5. Frequency-area statistics for failed clusters at the critical transition from nucleation to propagation. The cumulative numbers of clusters N_{cc} are given as a function of cluster area A_c for the four examples in Fig. 4. The straight lines are the correlation with the power-law scaling given in Eq. (32) taking $D = 4$. Colour version of this figure is available in electronic edition only.

In Figure 6 we give the dependence of the damage variable α on the nondimensional time t/t_0. Typical simulations are shown. There is some variability among simulations, but this is generally small, a few percent. The nucleation phase is delayed significantly as β is increased. This is expected since as $\beta \to \infty$ there will be no nucleation phase and the rupture will propagate at $t/t_0 = 1$. The nucleation phase has only a weak dependence on p. However, as p is increased the critical values of the damage variable α_c decrease.

In Figure 7a we give the dependence of the critical nondimensional failure time t_c/t_0 on the load sharing parameter p and in Fig. 7b we give the dependence of the corresponding critical damage parameter value α_c on p. In each case, we give results for $\beta = 2$, 6, and 10. We see that both t_c/t_0 and α_c decrease with increasing values of p.

We next determine the cumulative energy dissipated during fiber failures. During simulation, the nondimensional energy dissipated in a fiber failure E_f/E_0 is given by Eq. (28). These values are added to give the cumulative nondimensional energy dissipated E_f/E_0. These values are given as a function of nondimensional time t/t_0 in Fig. 8 for (a) $p = 0$, (b) $p = 0.5$, and (c) $p = 1.0$. In each case, results are given for $\beta = 2$, 6, and 10.

In Figure 9 we give the dependence of the ratio of energy generated in the nucleation phase E_n to the energy generated in the rupture phase E_r on the

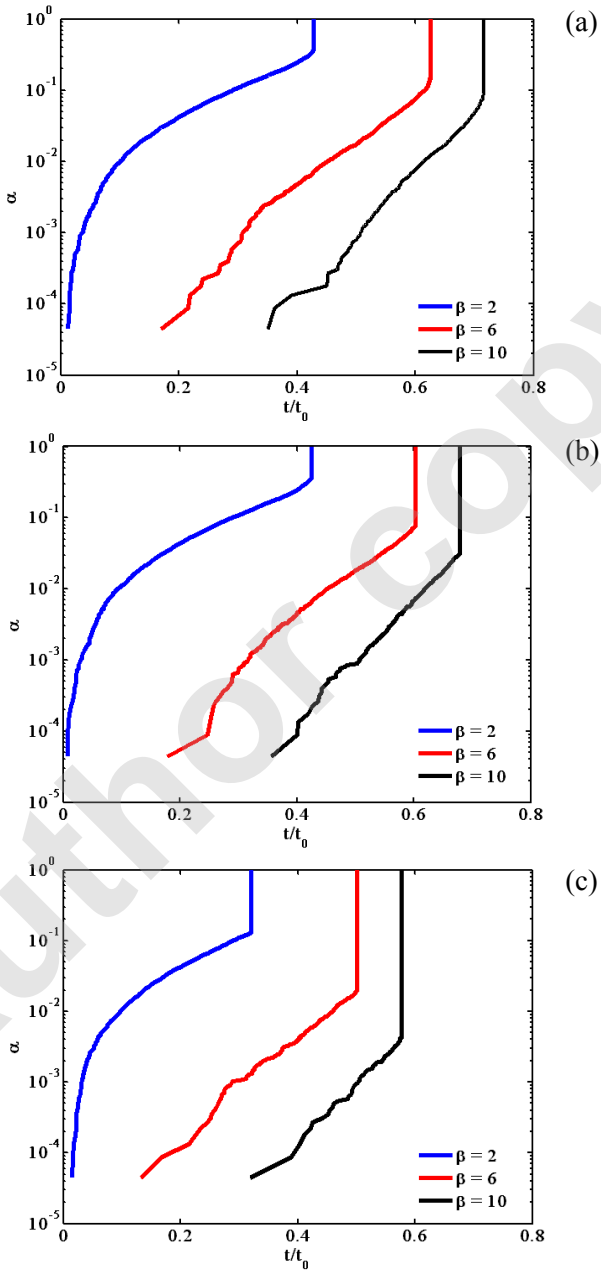

Fig. 6. Dependence of the damage variable α on the nondimensional time t/t_c. Results are given for: (a) $p = 0$, (b) $p = 0.5$, and (c) $p = 1.0$. In each case results are given for: $\beta = 2$, $\beta = 6$, and $\beta = 10$. The simulations given in (a) are basically identical to the analytical results given in Fig. 2.

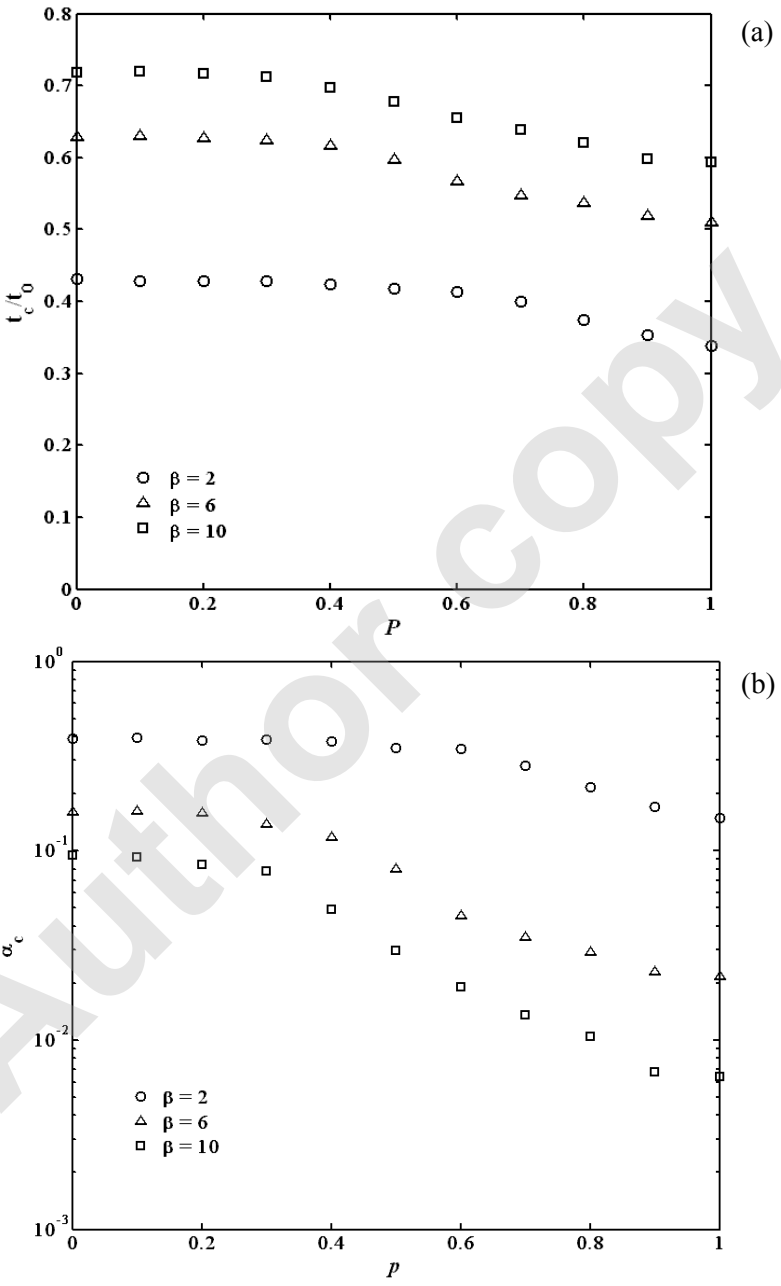

Fig. 7: (a) Dependence of the critical nondimensional failure time t_c/t_0 on the load sharing parameter p; (b) dependence of the corresponding critical damage parameters α_c on p. In both cases results are given for $\beta = 2$, 6, and 10.

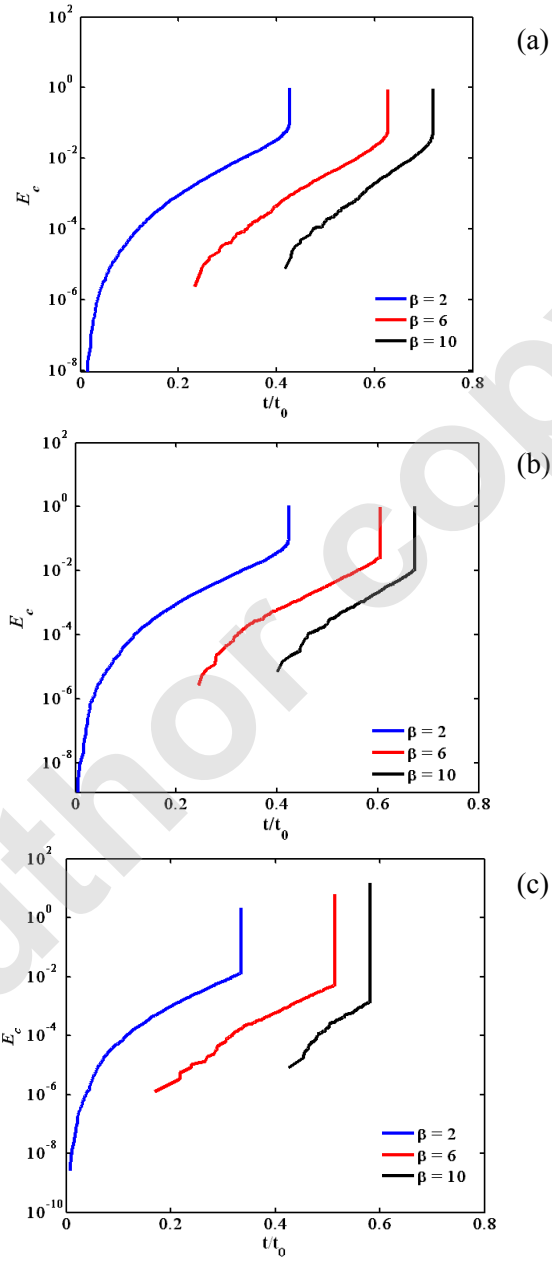

Fig. 8. Dependence of the nondimensional cumulative energy dissipated E_f/E_0 on the nondimensional time t/t_0. Results are given for: (a) $p = 0$, (b) $p = 0.5$, and (c) $p = 1.0$. In each case results are given for $\beta = 2$, 6, and 10. The simulations given in (a) are basically identical to the analytical results given in Fig. 3.

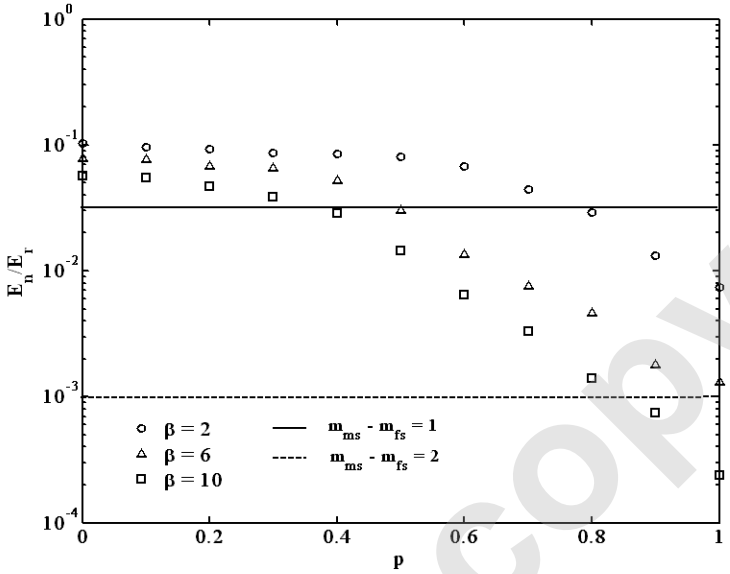

Fig. 9. Dependence of the ratio of energy generated in the nucleation phase E_n to the energy generated in the rupture phase E_r on the load sharing parameter p with $\beta = 2$, 6, and 10. We associate E_r with a main shock with magnitude m_{ms} and E_n with a single foreshock of magnitude m_{fs}. The energy ratios associated with $m_{ms} - m_{fs} = 1$ and 2 are all given.

load sharing parameter p with $\beta = 2$, 6, and 10. We associate the propagation phase with a main shock of magnitude m_{ms}, and we associate the nucleation phase with a single precursor earthquake of magnitude m_{fs}. Using the standard relation between earthquake energy and magnitude we write

$$\frac{E_n}{E_r} = 10^{-1.5(m_{ms} - m_{fs})} . \tag{33}$$

We also give in Fig. 9 energy ratios corresponding to $m_{ms} - m_{fs} = 1$ and 2.

A major focus of this paper is to study the role of precursory damage prior to a propagating rupture. The objective is to provide an explanation for the absence of small earthquakes as a precursor to the 2004 Parkfield earthquake as well as other earthquakes. Figure 9 illustrates the conditions under which precursory damage is reduced. For $p = 0$ (the uniform load sharing, mean-field limit) the energy in the precursory events is about 10% of the energy generated by the propagating rupture. There is only a weak dependence on the Weibull exponent β. The stress from a failed asperity is transferred to all other asperities. This transfer enhances precursory failures and a strong nucleation phase. We associate their behavior with the laboratory experi-

ments discussed above. The rigid granite blocks transfer the stress from a failed asperity across the entire saw cut (model fault).

For the $p = 1$ (local load sharing) limit the energy in the precursory damage is reduced considerably. There is also a strong dependence on the Weibull exponent β. With $\beta = 10$ and $p = 1$ the energy in the precursory events is only 0.02% of the energy in the propagating rupture. In order to relate our results to the problem of precursory seismic activity we have also included in Fig. 9 the magnitude of a single precursory earthquake that would give the fraction of precursory energy release during the nucleation phase. For p near unity and large β, the precursory single earthquake would have a magnitude two units less than the main shock associated with the propagation phase. For the 2004 Parkfield magnitude 6.0 earthquake this would be the energy associated with a single magnitude 4 earthquake.

With $p = 1$ the force from a failed asperity is transferred to adjacent asperities. This local transfer of stress accelerates fracture nucleation reducing precursory failures. We associate this behavior with faults. The matrix around a fault is heavily damaged and this damage inhibits the transfer of stress from a failed asperity over large distances.

5. DISCUSSION

A major problem in understanding earthquake physics is the absence of a precursory build up of seismicity associated with the rupture of a major earthquake. There was no evidence for precursory seismic activity prior to the 2004 Parkfield $M_w = 6$ earthquake. A very sensitive seismic array was located adjacent to the rupture and no systematic build up of activity was observed.

In order to study this problem, we have utilized a fiber-bundle model. Breaking fibers are hypothesized to be analogous to breaking asperities on a fault zone. The behavior of the fiber-bundle model is controlled by several parameters and assumptions. First we assume a "static" model in which failure forces on each fiber are specified. We believe that this is the appropriate approach for a model of a main shock since the build up of the tectonic stress is so slow. It is also necessary to specify the statistical distribution of failure stresses. We choose the Weibull distribution given in Eq. (3) because it is the accepted distribution for the failure of fiber bundle (Phoenix and Newman 2009). It is also necessary to specify the power-law exponent β of the distribution and we consider several values.

There are alternative ways in which the force on a failed fiber is redistributed. We introduce a redistribution parameter p which is the fraction of the force that is redistributed to neighboring fibers (local load sharing). The remainder of the force $1 - p$ is redistributed to all surviving fibers (uniform load sharing). It is also necessary to specify the range of local load sharing.

We assume that the fraction of the load p is redistributed to all surviving fibers in a square region with $2r + 1$ fibers on a side as defined in Eq. (7). When $2r + 1$ is equal to the size of the square grid of fibers local load sharing $p = 1$ is equivalent to equal load sharing and $p = 0$.

In our simulations we consider only local load sharing with $r = 1$. Our focus is on the role of parameters p and β on precursory failures. Our results are clearly illustrated in Fig. 9. Precursory failures are suppressed as $p \to 1$ for relatively large β. Local load sharing leads to a weak nucleation phase and a strong rupture phase. This result is clearly illustrated in Fig. 4. Precursory activity is very low for $p = 1$ and $\beta = 10$.

In the Appendix we have related the fiber-bundle model to the slider-block model. A slider-block model without healing is similar to the fiber-bundle model. When a block slips, it does not stick. The primary parameter in the slider-block model is the ratio of spring constants defined in Eq. (1). As shown in Eq. (A21), with very weak springs, $\gamma \to 0$, we have uniform load sharing corresponding to $p = 0$ in the fiber bundle model and with very strong connector springs, $\gamma \to \infty$, we have local load sharing corresponding to $p = 1$ in the fiber-bundle model. The redistribution parameter p plays the same role in the fiber-bundle model as the spring constant ratio γ in the slider-block model.

As discussed in the Introduction, the laboratory experiments on granite blocks carried out by Weeks *et al*. (1978) also exhibited systematic precursory acoustic emissions. Again it appears to be appropriate to associate these experiments with the uniform load sharing limit. The granite blocks behaved as loader plates in a slider-block model. When an asperity failed the rigid granite block transferred the force on that asperity to all surviving asperities.

We attribute the lack of precursory seismicity prior to earthquakes to local load sharing from failed asperities. The Earth's crust in seismogenic regions is populated by faults on all scales. This complexity allows the force on a failed asperity to be transferred only to neighboring asperities, *i.e*., local load sharing. Thus, the behavior of a fault is better approximated by the lack of precursory damage as illustrated in Fig. 4d.

APPENDIX

Slider-block model

There are strong similarities between the fiber-bundle model and the slider-block model. We will use these similarities to relate the load-sharing parameter p in our fiber-bundle model to the slider-block model. We consider

a slider-block model consisting of a two-dimensional square array of n_0 slider blocks pulled over a surface by a driver plate (Turcotte 1997). A constant pulling force F is applied to the driver plate. Each block is connected to the driver plate with a driver spring with spring constant K_L. Each block is connected to n_c adjacent blocks with connector springs with spring constants K_c. We assume that the blocks have a statistical distribution of static frictional failure strengths in analogy to the failure strengths of our fibers. The force F on the driver plate is increased from zero until the weakest block slips with a force F/n_0 on it. The extension of the connector springs x is given by

$$x = \frac{F}{n_0 K_L} . \tag{A1}$$

In order to relate the slider-block model to the fiber-bundle model we assume that the frictional force on the failed block is zero after slip.

To illustrate the behavior of this slider-block model we first consider two limiting cases: (1) no connector springs ($K_c = 0$) and (2) very strong connector springs ($K_c \gg K_L$). When a block fails with $K_c = 0$, there is no force on the block and the original force on the block xK_L is transferred equally to the $n - 1$ remaining blocks. This results in an increase in the extension of the loader springs from x to $x + \delta x$. The resulting force balance is

$$xK_L = (n-1) K_L \delta x , \tag{A2}$$

or

$$\delta x = \frac{x}{(n-1)} . \tag{A3}$$

With $K_c = 0$ and no frictional force on the failed block, the forces on the connector springs are zero so that the displacement of the failed block x_b is given by

$$x_b = x + \delta x = \frac{nx}{n-1} . \tag{A4}$$

This is the uniform-load sharing (mean field) limit. This corresponds to the $p = 0$ (uniform load sharing) limit for the fiber-bundle model.

When a block fails with $K_c \gg K_L$, the displacement of failed block is very small so that the force transmitted to this block through its loader spring remains unchanged. All loader springs transmit the same force so that there is no displacement of the driver plate and

$$\delta x = 0 . \tag{A5}$$

The load on the failed block is distributed uniformly to the n_c blocks to which it is connected by connector springs, this is local load sharing. The resulting force balance on the failed block requires

$$xK_L = n_c x_b K_c = n_c x_c K_c . \tag{A6}$$

The extension of the connector springs x_c is given by

$$x_c = \frac{xK_L}{n_c K_c} . \tag{A7}$$

In the limit $K_c/K_L \to \infty$ we have $x_b = x_c \to 0$. The load is redistributed locally and the driver plate does not move. This corresponds to the $p = 1$ (local load sharing) limit for the fiber-bundle model.

We now give the general result for arbitrary values of K_c and K_L. The force balance on the failed block before and after failure (slip) requires that

$$xK_L = (n-1)K_L \delta x + n_c K_c x_b . \tag{A8}$$

This reduces to Eqs. (A2) and (A6) in the appropriate limits. In addition, the static force balance between the force exerted by the driver spring and the force exerted by the n_c connector springs requires

$$\left(x + \delta x - x_b\right)K_L = n_c K_c x_b . \tag{A9}$$

Equations (A8) and (A9) can now be solved for the displacement of the loader plate δx and the displacement of the failed block x_b.

The displacement of the loader plate is given by

$$\delta x = \frac{K_L x}{n_c K_c n + K_L (n-1)} . \tag{A10}$$

This reduces to Eq. (A3) when $K_c = 0$ and to Eq. (A5) when $K_c \gg K_L$. The displacement of the failed block is given by

$$x_b = \frac{nK_L x}{n_c K_c n + K_L (n-1)} . \tag{A11}$$

This reduces to Eq. (A4) when $K_c = 0$ and to Eq. (A7) when $K_c \gg K_L$. We finally consider the partition of the load from a failed site to the surviving sites.

When a site fails the load f_f that is redistributed to other sites is given by

$$f_f = K_L x = f_{mf} + f_{LLS} , \tag{A12}$$

where f_{mf} is the fraction of the load redistributed uniformly (mean field) and f_{LLS} is the fraction of the load redistributed locally. The equal load sharing (mean field) component is redistributed to all surviving blocks due to the displacement δx of the drive plate. This component f_{mf} is given by

$$f_{mf} = (n-1)K_L \delta x \ , \tag{A13}$$

and using Eq. (A10) we obtain

$$f_{mf} = \frac{(n-1)K_L{}^2 x}{n_c K_c n + K_L(n-1)} \ . \tag{A14}$$

There is also a local load-sharing component that is redistributed to the n_c local blocks connected to the failed block by connector springs. This component f_{LLS} is given by

$$f_{LLS} = n_c x_b K_c \ , \tag{A15}$$

and using Eq. (A11) we obtain

$$f_{LLS} = \frac{n_c K_c n K_L x}{n_c K_c n + K_L(n-1)} \ . \tag{A16}$$

Adding Eqs. (A14) and (A16) gives (A12), as required.

We introduced the redistribution fraction in Eq. (7). Noting that

$$f_{LLS} = n_{rd} \Delta f_{lls} \ , \tag{A17}$$

and

$$f_f = f_{f\min} \ , \tag{A18}$$

we find

$$p = \frac{f_{LLS}}{f_f} \ . \tag{A19}$$

Introducing the ratio of spring constants defined in Eq. (1), substitution of Eqs. (A12) and (A16) in Eq. (A19) gives

$$p = \frac{n_c \gamma n}{n_c \gamma n + (n-1)} \ . \tag{A20}$$

For $n \gg 1$ we have

$$p = \frac{n_c \gamma}{n_c \gamma + 1} \ . \tag{A21}$$

This demonstrates that the local load sharing limit ($p = 1$) in the fiber bundle model corresponds to the $\gamma \to \infty$ ($K_c \gg K_L$) limit in the slider-block model and that the uniform (mean field) limit ($p = 0$) in the fiber-bundle model corresponds to the $\gamma = 0$ ($K_c = 0$) limit in the slider-block model.

Acknowledgements. YTL is grateful for research support from both the National Science Council (ROC) and the Institute of Geophysics (NCU, ROC). JBR was supported by USDoE grant DE-FG02-04ER15568.

References

Abramowitz, M., and I.A. Stegun (eds.) (1972), *Handbook of Mathematical Functions with Formulas, Graphs, and Mathematical Tables*, 9th ed., Dover Publications Inc., New York, 260 pp.

Alava, M.J., P.K.V.V. Nukala, and S. Zapperi (2006), Statistical models of fracture, *Adv. Phys*. **55**, 3-4, 349-476, DOI: 10.1080/00018730300741518.

Agnew, D.C., and L.M. Jones (1991), Prediction probabilities from foreshocks, *J. Geophys. Res*. **96**, B7, 11959-11971, DOI: 10.1029/91JB00191.

Bakun, W.H., B. Aagaard, B. Dost, W.L. Ellsworth, J.L. Hardebeck, R.A. Harris, C. Ji, M.J.S. Johnston, J. Langbein, J.J. Lienkaemper, A.J. Michael, J.R. Murray, R.M. Nadeau, P.A. Reasenberg, M.S. Reichle, E.A. Roeloffs, A. Shakal, R.W. Simpson, and F. Waldhauser (2005), Implications for prediction and hazard assessment from the 2004 Parkfield earthquake, *Nature* **437**, 969-974, DOI: 10.1038/nature04067.

Bowman, D.D., G. Ouillon, C.G. Sammis, A. Sornette, and D. Sornette (1998), An observational test of the critical earthquake concept, *J. Geophys. Res*. **103**, B10, 24359-24372, DOI: 10.1029/98JB00792.

Carlson, J.M., and J.S. Langer (1989), Mechanical model of an earthquake fault, *Phys. Rev. A* **40**, 11, 6470-6484, DOI: 10.1103/PhysRevA.40.6470.

Ciliberto, S., A. Guarino, and R. Scorretti (2001), The effect of disorder on the fracture nucleation process, *Physica D* **158**, 1-4, 83-104, DOI: 10.1016/S0167-2789(01)00306-2.

Coleman, B.D. (1958), Statistics and time dependence of mechanical breakdown in fibers, *J. Appl. Phys*. **29**, 6, 968-983, DOI: 10.1063/1.1723343.

Daniels, H.E. (1945), The statistical theory of the strength of bundles of threads, *Proc. Roy. Soc. A* **183**, 995, 405-435, DOI: 10.1098/rspa.1945.0011.

Garcimartin, A., A. Guarino, L. Bellon, and S. Ciliberto (1997), Statistical properties of fracture precursors, *Phys. Rev. Lett*. **79**, 17, 3202-3205, DOI; 10.1103/PhysRevLett.79.3202.

Guarino, A., A. Garcimartin, and S. Ciliberto (1998), An experimental test of the critical behavior of fracture precursors, *Eur. Phys. J. B* **6**, 13-24, DOI: 10.1007/s100510050521.

Guarino, A., S. Ciliberto, and A. Garcimartin (1999), Failure time and microcrack nucleation, *Europhys. Lett.* **47**, 4, 456-461, DOI: 10.1209/epl/i1999-00409-9.

Guarino, A., S. Ciliberto, A. Garcimartin, M. Zei, and R. Scorretti (2002), Failure time and critical behaviour of fracture precursors in heterogeneous materials, *Eur. Phys. J. B* **26**, 2, 141-151, DOI: 10.1140/epjb/e20020075.

Helmstetter, A., and D. Sornette (2003), Foreshocks explained by cascades of triggered seismicity, *J. Geophys. Res*. **108**, B10, 2457-2466, DOI: 10.1029/2003JB002409.

Hemmer, P.C., and A. Hansen (1992), The distribution of simultaneous fiber failures in fiber bundles, *J. Appl. Mech*. **59**, 4, 909-914, DOI: 10.1115/1.2894060.

Krajcinovic, D. (1996), *Damage Mechanics*, 2nd ed., Elsevier, Amsterdam, 761 pp.

Kun, F., S. Zapperi, and H.J. Herrmann (2000), Damage in fiber bundle models, *Eur. Phys. J. B* **17**, 2, 269-279, DOI: 10.1007/PL00011084.

Marone, C. (1998), Laboratory-derived friction laws and their application to seismic faulting, *Ann. Rev. Earth Planet. Sci*. **26**, 643-696, DOI: 10.1146/annurev.earth.26.1.643.

Meeker, W.Q., and L.A. Escobar (1998), *Statistical Methods for Reliability Data*, John Wiley and Sons, New York, 680 pp.

Phoenix, S.L., and W.I. Newman (2009), Time-dependent fiber bundles with local load sharing. II. General Weibull fibers, *Phys. Rev. E* **80**, 6, 066115, DOI: 10.1103/PhysRevE.80.066115.

Pradhan, S., A. Hansen, and B.K. Chakrabarti (2010), Failure processes in elastic fiber bundles, *Rev. Mod. Phys*. **82**, 1, 499-555, DOI: 10.1103/RevModPhys.82.499.

Pride, S.R., and R. Toussaint (2002), Thermodynamics of fiber bundles, *Physica A* **312**, 1-2, 159-171, DOI: 10.1016/S0378-4371(02)00816-6.

Reasenberg, P.A. (1999), Foreshock occurrence before large earthquakes, *J. Geophys. Res*. **104**, B3, 4755-4768, DOI: 10.1029/1998JB900089.

Savage, M.K., and D.M. dePolo (1993), Foreshock probabilities in the western Great-Basin eastern Sierra Nevada, *Bull. Seismol. Soc. Am.* **83**, 6, 1910-1938.

Scorretti, R., S. Ciliberto, and A. Guarino (2001), Disorder enhances the effects of thermal noise in the fiber bundle model, *Europhys. Lett.* **55**, 5, 626-632, DOI: 10.1209/epl/i2001-00462-x.

Turcotte, D.L. (1997), *Fractals and Chaos in Geology and Geophysics*, 2nd ed., Cambridge University Press, Cambridge, 398 pp.

Turcotte, D.L. (1999), Self-organized criticality, *Rep. Prog. Phys*. **62**, 10, 1377-1429, DOI: 10.1088/0034-4885/62/10/201.

Turcotte, D.L., S.G. Abaimov, R. Shcherbakov, and J.B. Rundle (2007), Nonlinear dynamics of nature hazards. **In:** A.A. Tsonis and J.B. Elsner (eds.), *Nonlinear Dynamics in Geosciences*, Springer, New York, 557-580, DOI: 10.1007/978-0-387-34918-3_30.

Weeks, J., D. Lockner, and J. Byerlee (1978), Change in b-values during movement on cut surfaces in granite, *Bull. Seismol. Soc. Am*. **68**, 2, 333-341.

Weibull, W. (1951), A statistical distribution function of wide applicability, *J. Appl. Mech.* **18**, 293-297.

Received 17 August 2011
Received in revised form 22 September 2011
Accepted 11 October 2011